ARTICLES
PUBLISHED ONLINE: 15 SEPTEMBER 2013 | DOI: 10.1038/NPHYS2735
nature physics

Observation of Majorana quantum critical behaviour in a resonant level coupled to a dissipative environment

H. T. Mebrahtu[1], I. V. Borzenets[1], H. Zheng[1], Y. V. Bomze[1], A. I. Smirnov[2], S. Florens[3], H. U. Baranger[1] and G. Finkelstein[1]*

A quantum phase transition is an abrupt change between two distinct ground states of a many-body system, driven by an external parameter. In the vicinity of the quantum critical point (QCP) where the transition occurs, a new phase may emerge that is determined by quantum fluctuations and is very different from either phase. In particular, a conducting system may exhibit non-Fermi-liquid behaviour. Although this scenario is well established theoretically, controllable experimental realizations are rare. Here, we experimentally investigate the nature of the QCP in a simple nanoscale system—a spin-polarized resonant level coupled to dissipative contacts. We fine-tune the system to the QCP, realized exactly on-resonance and when the coupling between the level and the two contacts is symmetric. Several anomalous transport scaling laws are demonstrated, including a striking non-Fermi-liquid scattering rate at the QCP, indicating fractionalization of the resonant level into two Majorana quasiparticles.

Quantum phase transitions (QPTs) are attracting strong interest in diverse fields of physics, ranging from quantum magnets and strongly correlated materials[1] to, more recently, cold atoms[2], nanostructures[3,4] and particle physics[5]. The foremost remarkable property of QPTs is the possibility to create exotic quantum states of matter at the QCP, such as deviations from the standard Fermi-liquid paradigm for metals. These zero-temperature states then cause anomalous physical properties at finite temperatures[1]. Another intriguing aspect of QPTs is their behaviour under non-equilibrium conditions, such as either a sudden quench driving the system non-adiabatically through the transition[6], or a strong perturbation provided by a large current density as typically realized in nanoelectronic devices[7]. Despite the ubiquity of QPTs in contemporary theoretical physics, obtaining clear experimental signatures has been challenging.

Here, we present a thorough characterization of all facets of a QPT in a fully tunable single-molecule transistor built from a spin-polarized carbon nanotube quantum dot connected to strongly dissipative contacts[8,9]. As the electronic level of the quantum dot crosses the Fermi energy of the leads, in the standard case of good metallic contacts transport occurs through a resonance of finite width and height. In contrast, the presence of dissipation drives the conductance to zero (in the limit of vanishing temperature), unless one tunes the position of the resonant level to the Fermi energy and simultaneously makes the tunnel barriers between the dot and the two leads perfectly equal. In the latter case, the conductance saturates at the unitary limit, e^2/h (e is the elementary charge and h is the Planck constant), and the resonance width tends to zero, as we recently demonstrated[9]. A quantum critical state is obtained, whose anomalous properties are the subject of the present study.

By optimizing the dissipative environment, we find that the quantum critical properties surprisingly behave very closely to the result for a bound single Majorana fermion mode, causing in particular a quasi-linear scattering rate in temperature T and voltage bias V. Majorana fermions are the subject of intense scrutiny in different contexts[10], ranging from particle physics[11] to topological insulators[12] and superconductors[13–15]. In our case, Majorana modes emerge owing to two strongly interacting leads attempting to hybridize with the resonant level: their competition results in only partial hybridization of the level with the continuum. The QCP then corresponds to a frustrated state in which a non-hybridized Majorana mode is generated, as predicted in the related context of the two-channel Kondo model[16,17].

The fabrication of the carbon nanotube quantum dot was described previously[8,9] (Fig. 1a). The device is operated in a magnetic field of $B = 3$ or 6 T and at electron temperatures down to $T = 50$ mK so that the quantum dot is effectively spin polarized. A key feature of our samples is that the coupling of the quantum dot to the left or right metallic lead can be varied independently using side gate voltages. We present data measured on two resonant levels during different experimental sessions, demonstrating compatible results.

Differential conductance maps ($G(V) \equiv \mathrm{d}I/\mathrm{d}V$) near one of these resonant peaks are shown in Fig. 2 for different degrees of coupling asymmetry. For asymmetric couplings, note the clear zero-bias anomaly (ZBA)—a suppressed conductance at zero bias for all gate values[18]. The ZBA is eliminated only for symmetric tunnel couplings and only exactly at the centre of the resonance (Fig. 2a). This sets the location of the QCP. These general observations[9] are summarized in Fig. 1b, which sketches a quantum critical diagram for our system: at zero temperature, the system is in a conducting state with conductance e^2/h at the QCP and in an insulating state otherwise. A generic feature of QPTs (ref. 1), which we

[1]Department of Physics, Duke University, Durham, North Carolina 27708, USA, [2]Department of Chemistry, North Carolina State University, Raleigh, North Carolina 27695, USA, [3]Institut Néel, CNRS and UJF, 25 avenue des Martyrs, BP 166, 38042 Grenoble, France. *e-mail: gleb@phy.duke.edu

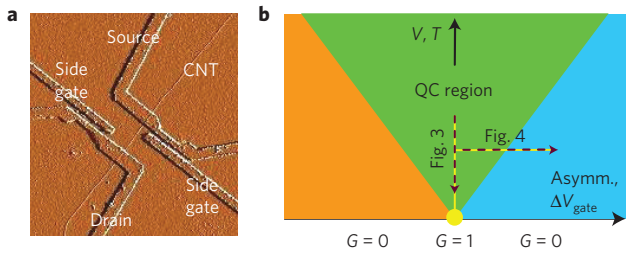

Figure 1 | Sample and schematic. a, Atomic force micrograph of a sample similar to the one measured. A single carbon nanotube is connected to long and resistive source and drain electrodes made of a thin Cr film. Tunnel barriers are tuned by two lateral side gates. **b**, A diagram of the QPT in our system. The control parameter (V_{gate} or tunnel barrier asymmetry) drives the system across the QCP with $G = 1$. Elsewhere, conductance tends to zero at $T = 0$. At finite temperatures, the influence of the QCP extends to the quantum critical (QC) region of finite width. We probe this region in several ways: the downward flow towards the QCP is considered in Fig. 3, whereas the runaway behaviour on gate detuning is investigated in Fig. 4.

now investigate in our device, is the existence of quantum critical correlations close to the QCP.

We first analyse the transport data taken with symmetric barriers and gate voltage tuned on-resonance, which corresponds to the vertical cross-section of Fig. 2a at $\Delta V_{gate} = 0$. In this case, perfect transmission survives down to the lowest temperature and zero-bias voltage. Figure 3a shows a series of conductance versus bias plots measured by stepping up the temperature. Strikingly, the conductance at the lowest temperatures shows a very unusual dependence on bias—a quasi-linear cusp. We replot $1 - G$ at the base temperature on a log–log scale in Fig. 3b. Clearly, the deviation of the zero-bias conductance from the unitary limit is quasi-linear: a fit to $1 - G \propto V^{\alpha}$ yields $\alpha \approx 1.1$. Essentially the same exponent $\alpha \approx 1.2$ is extracted from the T dependence of $1 - G$ (Fig. 3c). In the absence of dissipation in the leads, $1 - G$ usually scales with the conventional Fermi-liquid T^2 or V^2 dependence. Observation of a very different, intrinsically non-Fermi-liquid[16] exponent α underlines the striking role played by the dissipative environment.

To account for this behaviour, we draw on the analogy between tunnelling with dissipation (our experiment) and tunnelling in a Luttinger liquid—an interacting one-dimensional electronic system[16] that leads to violation of the Fermi-liquid paradigm. For tunnelling through a single barrier, this analogy was formally established in ref. 19 and used to understand experiments in ref. 20. We previously extended the analogy to the case of spinless resonant tunnelling[8,9] and will further use it here. (We stress that our experiment does not probe Luttinger-liquid physics in the nanotube: at this T, the length of an ideal, clean nanotube would have to be as large as 100 μm to suppress finite-size quantization.) In the bosonization language[16], the approach to the QCP is controlled by the leading irrelevant operator, $\cos(2\sqrt{\pi}\theta)\partial\theta$ (ref. 21), which corresponds to reflection of electron waves from the charge accumulated at the resonant level. On the basis of the scaling dimension of this operator, and transcribing the Luttinger

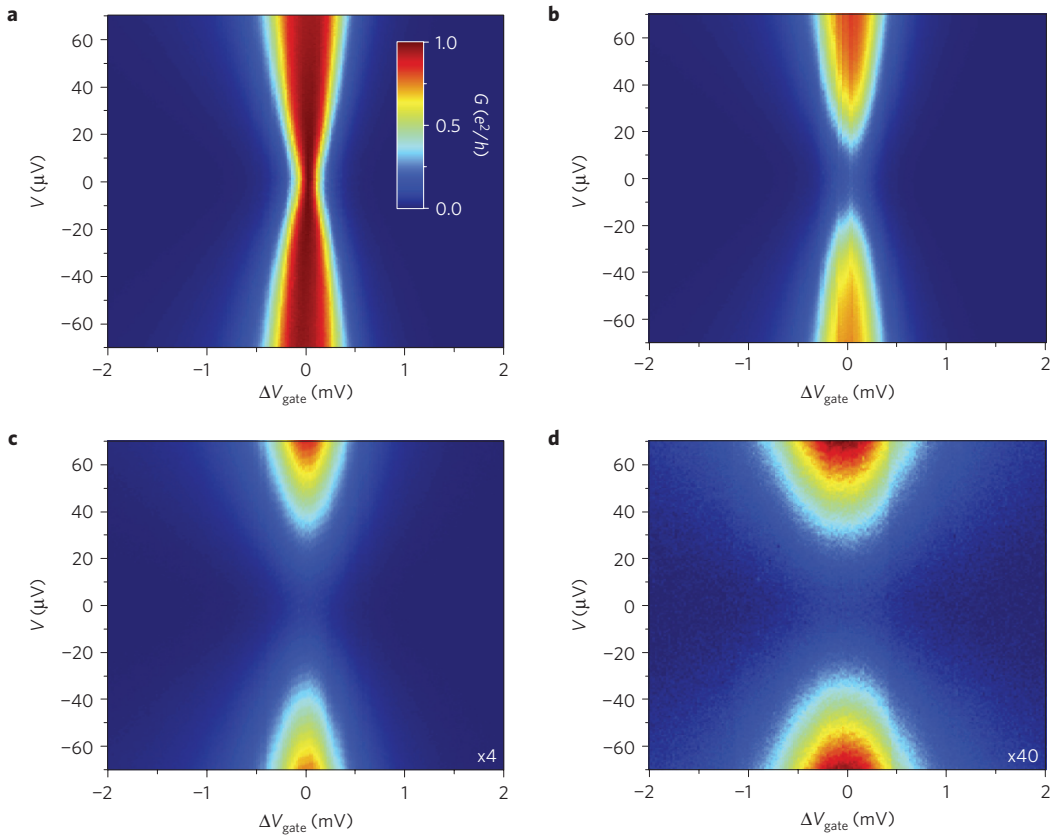

Figure 2 | Differential conductance maps close to the QCP. The maps are obtained by sweeping bias V and backgate offset voltage ΔV_{gate} (measured relative to the centre of the peak) at $T = 50$ mK and $B = 3$ T. **a**–**d**, Conductance in the symmetric case (**a**) is followed by maps showing progressively increasing barrier asymmetry in **b**–**d**, as controlled by the side gate voltages. The small conductance in **c**,**d** is multiplied by ×4 and ×40, respectively, to improve its visibility. The colour scale in **a** applies to all panels. Throughout this Article, we express the differential conductance G in units of $e^2 = h$. The prominent ZBA in the asymmetric cases completely disappears when symmetric and on resonance, indicating a QPT.

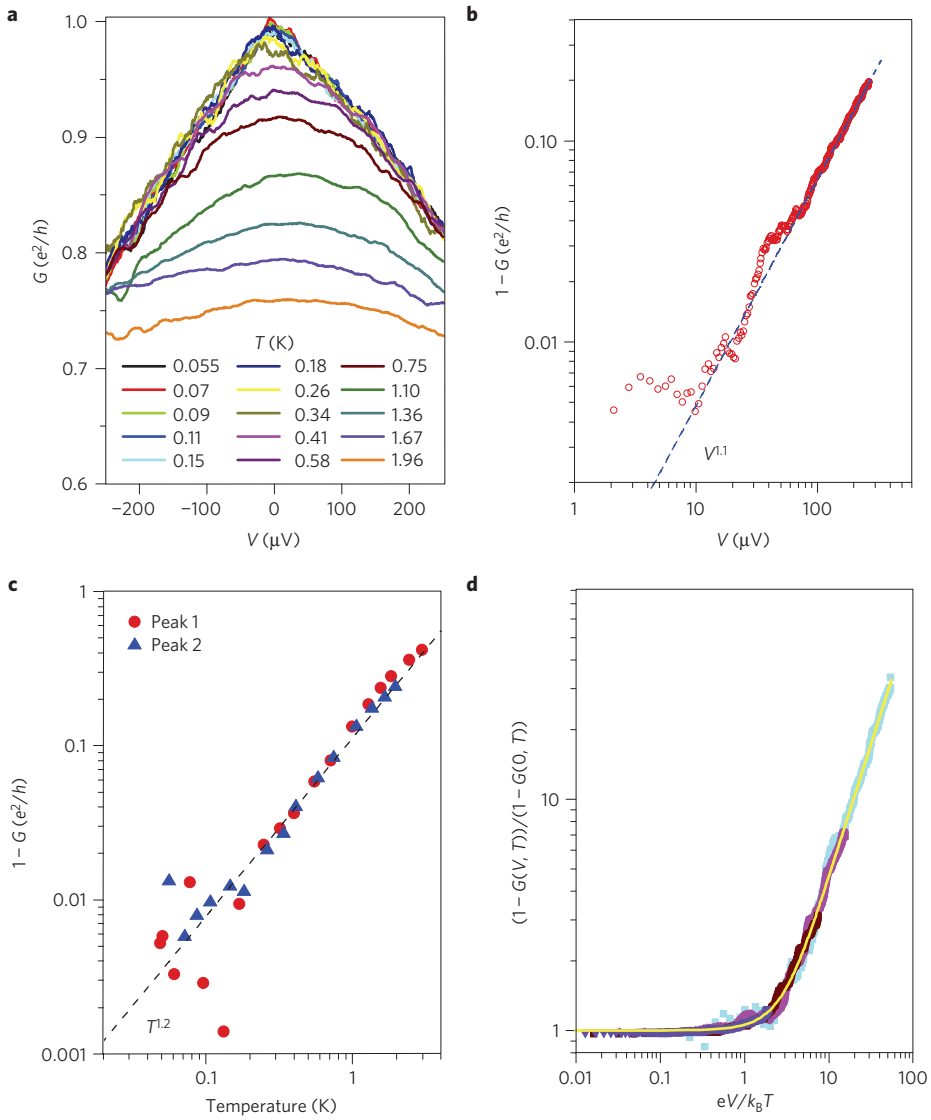

Figure 3 | Critical flow. a, Nonlinear conductance $G(V,T)$ at the QCP ($\Delta V_{gate}=0$ and symmetric barriers) measured at increasing temperatures. The quasi-linear behaviour at low T signals the presence of a Majorana state. **b**, $1-G$ measured versus bias voltage V at $T=55$ mK (symbols). The dashed line is a best fit to a power law $1-G\propto V^{\alpha}$, excluding the range $eV<k_BT$ where the conductance saturates. **c**, Deviation of zero-bias conductance from the unitary limit $1-G$ at the QCP as a function of temperature. Different symbols correspond to two different Coulomb blockade peaks measured on the same sample; the dashed line is a best fit to Peak 2, giving an exponent $\alpha=1.2$. **d**, A representative set of conductance curves from **a** at four different temperatures, plotted as $1-G(V,T)$ normalized by $1-G(0,T)$. A line fit (yellow, see text) is superimposed on the data (symbols, see legend in **a**). The collapse of the data onto a single curve as a function of eV/k_BT demonstrates the universality produced by proximity to the QCP.

interaction parameter g to the dimensionless dissipation strength r according to $g=1/(r+1)$ (refs 9,19), we expect the approach to the unitary limit to follow $1-G\propto T^{2/(r+1)}$ (refs 21,22). For this sample, the strength of the dissipation is $r\approx 0.75$ (or $g\approx 0.57$), as measured from the ZBA far off resonance[9]. The predicted quantum critical exponent, $2/(r+1)\approx 1.14$, is thus very close to the value of α found experimentally (Fig. 3b,c), demonstrating the ability of the Luttinger framework to explain our data.

The analogy between tunnelling with dissipation and tunnelling in a Luttinger liquid provides further insight into the microscopic nature of the quantum critical state. In the Luttinger-liquid case, it is known that for $g=1/2$ the resonant level can be mapped[23] onto the quantum critical two-channel Kondo Hamiltonian[3,16,17]. The latter may in turn be understood in terms of a hybridization of the leads with only half of the spinless fermion residing on the resonant level, leaving a fractional degeneracy associated with the remaining non-hybridized single Majorana mode[17]. Using this intuition, we directly map our problem for $r=1$ and on-resonance ($\Delta V_{gate}=0$) onto the following effective Hamiltonian:

$$\begin{aligned} H_{\text{Majorana}} &= (V_S-V_D)\left[\hat{\psi}_f^{\dagger}(x=0)-\hat{\psi}_f(x=0)\right]\hat{a} \\ &+ i(V_S+V_D)\left[\hat{\psi}_f^{\dagger}(x=0)+\hat{\psi}_f(x=0)\right]\hat{b} \\ &- 2\pi i v_F \hat{\psi}_c^{\dagger}(x=0)\hat{\psi}_c(x=0)\hat{a}\hat{b} \end{aligned} \quad (1)$$

Here, $\hat{a}$ and $\hat{b}$ are the two Majorana modes that describe a single fermion on the dot, $\hat{d}^{\dagger}=\hat{a}-i\hat{b}$, and $\hat{\psi}_{c/f}(x)$ are two extended fermionic fields that incorporate in a non-trivial way the electronic degrees of freedom of the leads and the electromagnetic phase fluctuations in the circuit (Supplementary Information).

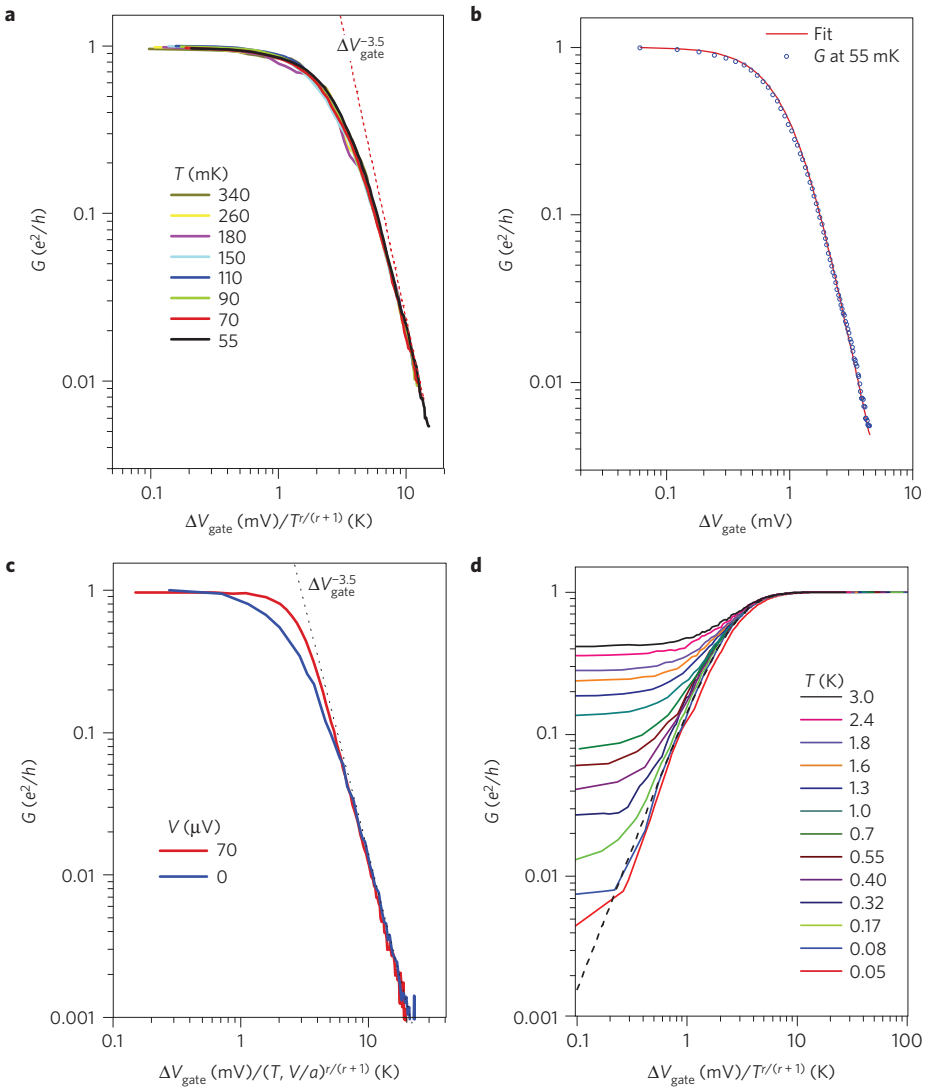

Figure 4 | Runaway flow. a, Resonant peak conductance as a function of the one-parameter scaling variable $X = \Delta V_{gate}/T^{r/(r+1)}$. Several curves measured at eight different temperatures between 55 and 340 mK scale to the same universal curve. **b**, Single-parameter scaling function extracted from **a** compared with the universal single-barrier scaling curve, equation (2), predicted in ref. 32. A good fit is achieved by optimizing a single fitting parameter, namely a dimensionless prefactor accompanying X. (For clarity, we plot only the data measured at the lowest temperature.) **c**, Comparison of the peak shape measured at finite T under equilibrium ($eV \ll k_B T$) and non-equilibrium ($eV \gtrsim k_B T$) conditions. The horizontal axis is $X = \Delta V_{gate}/T^{r/(r+1)}$ in the former case and $X = \Delta V_{gate}/(V/A)^{r/(r+1)}$ in the latter (for the value of constant A, see the main text). The power laws near zero conductance and near perfect transparency are the same, but a substantial difference between the two curves develops in the crossover region. **d**, Behaviour of $1-G$ near the peak conductance at several temperatures. The dashed line corresponds to the result of equation (2), which scales as $\sim X^2$ for small X. In each experimental curve, the change from saturation to $\sim X^2$ behaviour marks the range associated with the QCP. Thus, the quantum critical region (Fig. 1) is mapped out.

One of the Majorana modes, $\hat{b}$, is hybridized and dissolves into the continuum. For symmetric coupling $V_S = V_D$, the first term in equation (1) is eliminated, and the other mode, $\hat{a}$, is not hybridized, allowing for the existence of an independent Majorana mode on the dot. The density–density interaction (last term in equation (1)) does not destroy this independence[24,25]; however, this strong interaction (of the order of the Fermi energy) does govern the transport properties near the critical point. We show that perturbative treatment[24–26] of this interaction yields an anomalous linear-in-temperature dependence, $1 - G \propto T^1$ (Supplementary Information). Note that this result is different from the $\propto T^{1/2}$ dependence found in the two-channel Kondo effect[3]; indeed, the current operator is different in the two problems.

This striking deviation from Fermi-liquid theory follows from the qualitative difference in the correlations of the hybridized and independent Majorana modes: without the third term in equation (1), the correlations of the hybridized Majorana fermion decrease at long times, $\langle \hat{b}^\dagger(0)\hat{b}(t)\rangle \propto 1/t$, whereas those of the non-hybridized mode do not decay, $\langle \hat{a}^\dagger(0)\hat{a}(t)\rangle \propto 1$. This lack of decay reduces the exponent from the Fermi-liquid result $1-G \propto T^2$ to $\propto T^1$. We conclude that the almost linear approach to the unitary conductance observed in Fig. 3 signals the presence of a Majorana-like state. Our experiment thus demonstrates a route to using quantum criticality to tailor exotic electronic states in nanodevices.

An important feature of our experiment is the possibility to perturb the quantum critical state by out-of-equilibrium effects, namely in the presence of a finite voltage bias. We have already seen in Fig. 3c that the dependences of $1-G$ on T and V feature the same exponent α. Interestingly, the set of curves in Fig. 3a associated with the low-temperature, low-bias approach to the QCP can be rescaled onto a single universal curve, by plotting $(1-G(V \neq 0, T))/(1-G(V=0,T))$ versus $eV/k_B T$ (Fig. 3d). The

solid line is a numerical derivative of the heuristic expression $V|(\Gamma(\alpha/2+1+ieV/2\pi k_B T))/(\Gamma(1+ieV/2\pi k_B T))|^2$ with respect to V, properly normalized to 1 at $V=0$. This scaling function describes the experimental data without any fitting parameters, as we use the previously determined exponent $\alpha \equiv 2/(r+1)$. This form of the scaling function is inspired by the universal scaling of $(G(V\neq 0,T))/(G(V=0,T))$ in the regime of vanishing conductance (away from resonance), which is given by the same functional expression with α replaced by $2r$ (ref. 9). Although the scaling at weak coupling is theoretically well established[27], the scaling at the QCP, first reported here, still requires formal justification. We note that the similar behaviours of G for the weak coupling and $1-G$ for strong coupling cannot be explained by duality of the reflection and the transmission at the corresponding fixed points[28]–indeed, the two limiting behaviours are determined by different operators.

We now turn to the runaway behaviour from the QCP towards the zero-conductance state caused by a backgate offset voltage $\Delta V_{\rm gate}$, as sketched in Fig. 1b. We focus on the shape of the resonant peak as a function of gate voltage and temperature or bias. In Fig. 4a, the peak shape is plotted as a function of the single parameter $X=\Delta V_{\rm gate}/T^{r/(r+1)}$ (refs 28,29). Clearly, the data sets measured at different temperatures collapse onto a single universal curve $G(X)$. Importantly, this scaling applies not only for high values of conductance comparable to e^2/h (as captured by the resonance width at half height[9]), but also to relatively large values of X where $G \ll 1$. The scaling thereby describes the full runaway flow from the strongly coupled QCP to the weakly coupled regime. Such single-parameter scaling has been conjectured for resonant tunnelling in the Luttinger liquid in ref. 28, where the double-barrier structure is treated as a single barrier with a gate-tunable transparency. The validity of this assumption has been analysed for weak interactions[30,31]; our results further corroborate the single-parameter scaling in the strongly interacting case ($r\sim 1$).

Concentrating first on the low-conductance tail obtained for large backgate detuning $X \gg 1$, we obtain $G \propto (\Delta V_{\rm gate})^{-\beta}$ with an exponent $\beta \simeq 3.4$ (Fig. 4c). This is very close to the value $2(r+1)\approx 3.5$ expected from the analogy to tunnelling in a Luttinger liquid[28,29]. This result is markedly different from the usual tail of the Lorentzian line shape, $G \propto (\Delta V_{\rm gate})^{-2}$, expected for resonant tunnelling without dissipation.

To further examine the assumption of single-barrier-like scaling, we compare the universal scaling curve obtained in the experiment to the recent non-perturbative renormalization group calculations for single-barrier tunnelling in a Luttinger liquid[32] (Fig. 4b). Thus, we use the following ansatz for the full crossover function describing the equilibrium conductance G as a function of both detuning and temperature:

$$\frac{T}{T^{\star}[\Delta V_{\rm gate}]} = \frac{(G/G_0)^{1/2r}}{(1-G/G_0)^{(1+r)/2r}}\sqrt{\frac{1+rG/G_0}{1+r}} \qquad (2)$$

with $G_0 = e^2/h$ and $T^{\star}[\Delta V_{\rm gate}] \propto (\Delta V_{\rm gate})^{(1+r)/r}$. The excellent agreement between the experimentally determined scaling function and the full runaway curve of equation (2) (Fig. 4b) justifies the use of the single-barrier expressions to describe the scaling of the double-barrier system away from the resonance.

Applying a finite bias brings further insight by allowing us to probe the relation between equilibrium and non-equilibrium scaling (Fig. 4c). For the Luttinger-liquid system, analysis near the decoupled fixed point[28] predicts that the temperature scaling and bias scaling are proportional: $b_T/b_V = \pi^{2r}[\Gamma(1+r)]^2$, where $G(T=0,V)\simeq b_V(eV)^{2r}$ at small bias and $G(T,V=0)\simeq b_T(k_B T)^{2r}$ at low temperature. Thus, if we form a scaling curve using V in place of T, the two scaling curves should collapse onto each other in the small conductance limit if eV is divided by $A \equiv \pi[\Gamma(1+r)]^{1/r}k_B \simeq 2.8k_B$ for $r=0.75$. The data in Fig. 4c demonstrate that this holds for our system. However, the full scaling curves are clearly quite different: although they show, as expected[28], the same power laws close to both the strong and weak coupling fixed points, the bias scaling function makes a substantially sharper transition between the two. To the best of our knowledge, there is no firm theoretical prediction for the full crossover curve of nonlinear conductance at arbitrary values of the dissipation parameter r.

Finally, quantum critical correlations are expected[1] to exist away from the critical point for temperatures larger than a characteristic gate-dependent scale (Fig. 1). Experimentally, we can define the boundary of the quantum critical region from the behaviour of $1-G$ near the peak conductance. On general grounds, a dissipation-independent exponent $1-G \propto (\Delta V_{\rm gate})^2$ is expected from the assumption of single-barrier scaling[28], resulting in a universal $1-G \propto X^2 \equiv [\Delta V_{\rm gate}/T^{r/(r+1)}]^2$ dependence at small X. This behaviour is indeed observed at low enough temperatures in Fig. 4d for $X \sim 1\,{\rm meV/K}^{0.43}$. However, the approach of $1-G$ to 0 is cut off near the QCP by the leading irrelevant operator, causing $1-G$ to saturate at small X. (More directly, the effect of the leading irrelevant operator is seen in the power laws of Fig. 3.) Thereby, the saturation delineates the quantum critical region; indeed, notice that the width of the saturation region gets progressively narrower as the temperature is reduced. We may define the width of the quantum critical region in $\Delta V_{\rm gate}$ by comparing the small corrections to full transparency due to the relevant operator $\propto [\Delta V_{\rm gate}/T^{r/(r+1)}]^2$ (Fig. 4) to those due to the leading irrelevant operator $\propto T^{2/(r+1)}$ (Fig. 3). The quantum critical region defined in this way has a simple shape: $\Delta V_{\rm gate} \propto T$. We convert $\Delta V_{\rm gate}$ to the actual energy position of the level $\Delta\epsilon_d$ by multiplying by the experimentally determined gate efficiency factor of about 0.2. We then find $\Delta\epsilon_d/k_B T \simeq 1$, indicating that the boundary of the quantum critical region simply corresponds to the centre of the conductance peak being shifted away from the Fermi energy by $\sim k_B T$. Although seemingly natural, this result is not obvious a priori, because the width of the resonant peak is much larger than $k_B T$ and scales as a non-trivial power of temperature.

We presented a comprehensive study of the QPT in a resonant level subject to finite dissipation, explicitly demonstrating the consistency of various scaling laws based on the Luttinger-liquid analogy. This allowed us to identify the QCP as closely related to a single Majorana bound state, with a scattering rate quasi-linear in temperature. Although our device, which requires fine-tuning of several gates and a carefully crafted dissipative environment, is not likely to provide a useful platform for Majorana-based quantum computing[33], it certainly allows one to explore fascinating Majorana physics in the presence of strong correlations, reaching regimes that may be harder to achieve in topological circuits.

Received 16 December 2012; accepted 24 July 2013; published online 15 September 2013

References

1. Sachdev, S. *Quantum Phase Transitions* 2nd edn (Cambridge Univ. Press, 2011).
2. Bloch, I., Dalibard, J. & Nascimbène, S. Quantum simulators with ultracold quantum gases. *Nature Phys.* **8,** 267–276 (2012).
3. Potok, R. M., Rau, I. G., Shtrikman, H., Oreg, Y. & Goldhaber-Gordon, D. Observation of the two-channel Kondo effect. *Nature* **446,** 167–171 (2007).
4. Roch, N., Florens, S., Bouchiat, V., Wernsdorfer, W. & Balestro, F. Quantum phase transition in a single-molecule quantum dot. *Nature* **453,** 633–637 (2008).
5. Cubrovic, M., Zaanen, J. & Schalm, K. String theory, quantum phase transitions and the emergent Fermi-liquid. *Science* **325,** 439–444 (2009).
6. Zurek, W. H., Dorner, U. & Zoller, P. Dynamics of a quantum phase transition. *Phys. Rev. Lett.* **95,** 105701 (2005).
7. Chung, C-H., Le Hur, K., Vojta, M. & Wölfle, P. Non-equilibrium transport at a dissipative quantum phase transition. *Phys. Rev. Lett.* **102,** 216803 (2009).
8. Bomze, Yu., Mebrahtu, H., Borzenets, I., Makarovski, A. & Finkelstein, G. Resonant tunneling in a dissipative environment. *Phys. Rev. B* **79,** 241402(R) (2009).

9. Mebrahtu, H. T. *et al.* Quantum phase transition in a resonant level coupled to interacting leads. *Nature* **488,** 61–64 (2012).
10. Wilczek, F. Majorana returns. *Nature Phys.* **5,** 614–618 (2009).
11. Avignone, F. T., Elliott, S. R. & Engel, J. Double beta decay, Majorana neutrinos, and neutrino mass. *Rev. Mod. Phys.* **80,** 481–516 (2008).
12. Hasan, M. Z. & Kane, C. L. Colloquium: Topological insulators. *Rev. Mod. Phys.* **82,** 3045–3067 (2010).
13. Mourik, V. *et al.* Signatures of Majorana fermions in hybrid superconductor–semiconductor nanowire devices. *Science* **336,** 1003–1007 (2012).
14. Rokhinson, L. P., Liu, X. & Furdyna, J. K. The fractional a.c. Josephson effect in a semiconductor–superconductor nanowire as a signature of Majorana particles. *Nature Phys.* **8,** 795–799 (2012).
15. Das, A. *et al.* Zero-bias peaks and splitting in an Al–InAs nanowire topological superconductor as a signature of Majorana fermions. *Nature Phys.* **8,** 887–895 (2012).
16. Giamarchi, T. *Quantum Physics in One Dimension* (Oxford Univ. Press, 2004).
17. Emery, V. J. & Kivelson, S. Mapping of the two-channel Kondo problem to a resonant-level model. *Phys. Rev. B* **46,** 10812–10817 (1992).
18. Ingold, G-L. & Nazarov, Yu. V. in *Single Charge Tunneling: Coulomb Blockade Phenomena in Nanostructures* (eds Grabert, H. & Devoret, M. H.) 21–107 (Plenum Press, 1992).
19. Safi, I. & Saleur, H. One-channel conductor in an ohmic environment: Mapping to a Tomonaga-Luttinger liquid and full counting statistics. *Phys. Rev. Lett.* **93,** 126602 (2004).
20. Jezouin, S. *et al.* Tomonaga-Luttinger physics in electronic quantum circuits. *Nature Commun.* **4,** 1–8 (2013).
21. Eggert, S. & Affleck, I. Magnetic impurities in half-integer-spin Heisenberg antiferromagnetic chains. *Phys. Rev. B* **46,** 10866–10883 (1992).
22. Meden, V., Enss, T., Andergassen, S., Metzner, W. & Schönhammer, K. Correlation effects on resonant tunneling in one-dimensional quantum wires. *Phys. Rev. B* **71,** 041302(R) (2005).
23. Komnik, A. & Gogolin, A. O. Resonant Tunneling between Luttinger liquids: A solvable case. *Phys. Rev. Lett.* **90,** 246403 (2003).
24. Sengupta, A. M. & Georges, A. Emery-Kivelson solution of the two-channel Kondo problem. *Phys. Rev. B* **49,** 10020–10022 (1994).
25. Coleman, P., Ioffe, L. B. & Tsvelik, A. M. Simple formulation of the two-channel Kondo model. *Phys. Rev. B* **52,** 6611–6627 (1995).
26. Zitko, R. Detection of Majorana edge states in topological superconductors through non-Fermi-liquid effects induced in an interacting quantum dot. *Phys. Rev. B* **83,** 195137 (2011).
27. Zheng, W., Friedman, J. R., Averin, D. V., Han, S. Y. & Lukens, J. E. Observation of strong Coulomb blockade in resistively isolated tunnel junctions. *Solid State Commun.* **108,** 839–843 (1998).
28. Kane, C. L. & Fisher, M. P. A. Transmission through barriers and resonant tunneling in an interacting one-dimensional electron gas. *Phys. Rev. B* **46,** 15233–15262 (1992).
29. Furusaki, A. & Nagaosa, N. Resonant tunneling in a Luttinger liquid. *Phys. Rev. B* **47,** 3827–3831 (1993).
30. Nazarov, Yu. V. & Glazman, L. I. Resonant tunneling of interacting electrons in a one-dimensional wire. *Phys. Rev. Lett.* **91,** 126804 (2003).
31. Polyakov, D. G. & Gornyi, I. V. Transport of interacting electrons through a double barrier in quantum wires. *Phys. Rev. B* **68,** 035421 (2003).
32. Aristov, D. N. & Wölfle, P. Transport of interacting electrons through a potential barrier: Nonperturbative RG approach. *Europhys. Lett.* **82,** 1–6 (2008).
33. Nayak, C., Simon, S. H., Stern, A., Freedman, M. & Das Sarma, S. Non-Abelian anyons and topological quantum computation. *Rev. Mod. Phys.* **80,** 1083–1159 (2008).

Acknowledgements

We appreciate valuable discussions with I. Affleck, C. H. Chung, P. Coleman, K. Ingersent, K. Le Hur and P. A. Lee. We thank J. Liu for providing the nanotube growth facilities and W. Zhou for helping to optimize the nanotube synthesis. H.Z., S.F. and H.U.B. thank the Fondation Nanosciences de Grenoble for facilitating the exchange between Grenoble and Duke. The work in the US was supported by US DOE awards DE-SC0002765, DE-SC0005237 and DE-FG02-02ER15354.

Author contributions

H.T.M., I.V.B. and G.F. designed the experiment. H.T.M. fabricated the samples. H.T.M., I.V.B., Y.V.B., A.I.S. and G.F. conducted the experiment. H.T.M., H.Z., S.F., H.U.B. and G.F. analysed and interpreted the data. H.Z., S.F. and H.U.B. developed the theory.

Additional information

Supplementary information is available in the online version of the paper. Reprints and permissions information is available online at www.nature.com/reprints. Correspondence and requests for materials should be addressed to G.F.

Competing financial interests

The authors declare no competing financial interests.